Fire Safety Journal 106 (2019) 13–28

Contents lists available at ScienceDirect

Fire Safety Journal

journal homepage: www.elsevier.com/locate/firesaf

ANN models for prediction of residual strength of HSC after exposure to elevated temperature

Husain Abbas, Yousef A. Al-Salloum*, Hussein M. Elsanadedy, Tarek H. Almusallam

Chair of Research and Studies in Strengthening and Rehabilitation of Structures, Dept. of Civil Engineering, College of Engineering, King Saud University, P.O. Box 800, Riyadh, 11421, Saudi Arabia

ARTICLE INFO

Keywords:
High-strength concrete (HSC)
Elevated temperature
Compressive strength
ANN
Residual strength
Fire

ABSTRACT

Although high strength concrete (HSC) is becoming popular in building construction around the globe, its performance under high temperature (or fire) exposure is not precisely known. The existing fire-design provisions were developed mostly from the results of fire tests on normal strength concrete (NSC) and thus their applicability to HSC needs to be evaluated because sufficient HSC data is now available. This paper is aimed at developing artificial neural network (ANN) based predictive relationships between the statistically significant parameters and the residual compressive strength of concrete for its application in structural fire design of HSC. The proposed models are based on a large set of experimental data that was collected through an extensive survey of the available tests on HSC after high-temperature exposure. The data was carefully examined and analyzed to identify the statistically significant/sensitive variables and to establish the influence of these variables on the residual strength of HSC. The database was used to check the validity/applicability of the existing design models of codes, standards, guidelines and several researchers. New ANN based residual strength design models for HSC were also proposed.

1. Introduction

The use of high-strength concrete (HSC) for structural components, is becoming exceedingly common in the Kingdom of Saudi Arabia as well as the rest of the world. A number of structures including bridges are being constructed with HSC or high performance concretes (HPC) with strengths exceeding 60 MPa, due to the number of advantages offered by such concretes [1]. Although there is no precise point of separation between HSC and normal-strength concrete (NSC), the ACI 363R-10 [2] defines HSC as concrete with compressive strength over 6000 psi (41.4 MPa). This definition is adopted in this paper to distinguish between HSC and NSC data.

HSC has many advantages due to which its use in the construction industry is ever increasing all over the world. This is due to such better physico-mechanical properties as compressive strength, stiffness, and long-term durability and also due to the economic gains, which can be achieved with reductions in geometrical sections and gain in the architectural space to be exploited. Hence, technical, economic as well as aesthetic criteria favor the use of HSC over NSC [3].

It is well established that the mechanical properties of concrete are adversely affected by high-temperature exposure [4–14]. Mechanical properties of concrete at elevated temperature are determined by testing plain concrete specimens using one of three types of steady-state temperature tests (see Fig. 1): *stressed* tests, *unstressed* tests, and *unstressed residual property* tests [15]. Briefly, in *stressed* tests, a preload (20–40% of the room temperature compressive strength) is applied to the specimen before heating and is sustained during heating. Heat is applied at a constant rate until a target temperature T is reached, and is maintained for a time t until a thermal steady state is achieved. Stress or strain is then increased at a prescribed rate until the specimen fails. In *unstressed* tests, the specimen is heated, without preload, at a constant rate to the target temperature, which is maintained until a thermal steady state is achieved. Stress or strain is then applied at a prescribed rate until failure occurs. In *unstressed residual property* tests, the specimen is heated without preload at a prescribed rate to the target temperature, which is maintained until a thermal steady state is achieved. The specimen is then allowed to cool, at a prescribed rate, to room temperature. Subsequently, the specimen is tested at room temperature under axial compression until failure.

The studies on the effects of elevated temperature exposure on engineering properties of concrete [16–25] concluded that the behavior of HSC at high temperature differs from that of NSC under the same heating condition. NSC typically loses between 10 and 20% of its original compressive strength when heated to 300 °C, and between 60 and

* Corresponding author.
E-mail address: ysalloum@ksu.edu.sa (Y.A. Al-Salloum).

https://doi.org/10.1016/j.firesaf.2019.03.011
Received 11 November 2018; Received in revised form 11 March 2019; Accepted 27 March 2019
Available online 01 April 2019
0379-7112/

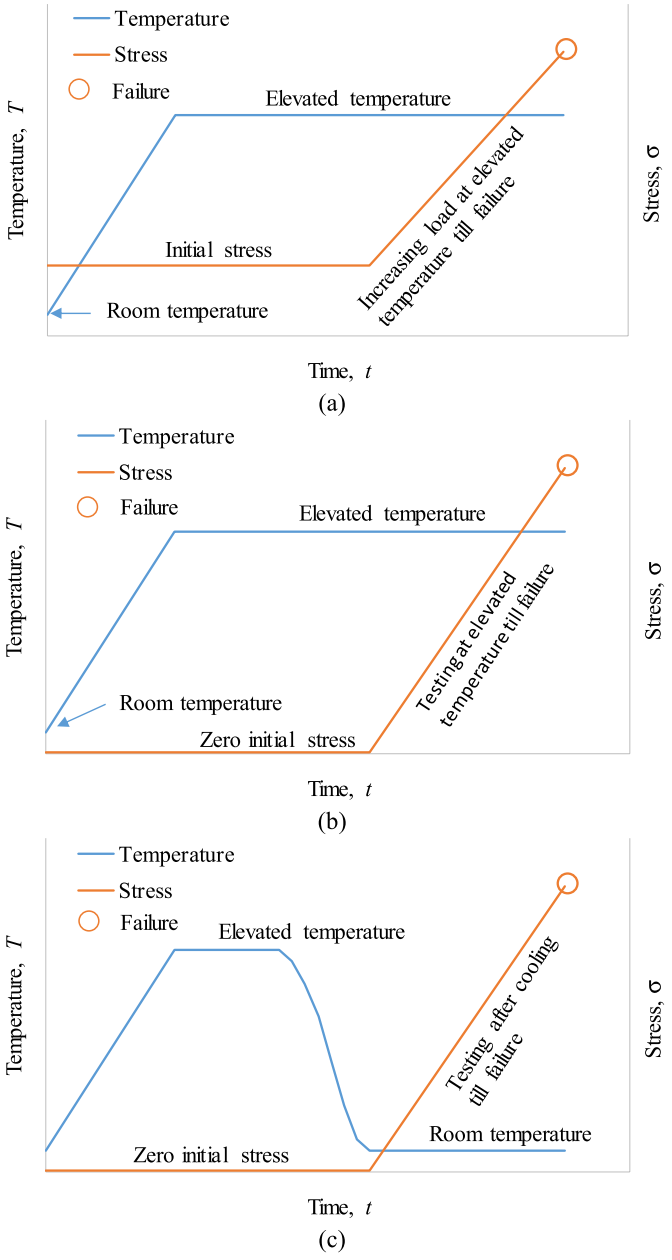

Fig. 1. Schematic of temperature and loading histories for the different test methods: (a) Stressed test: Initially stressed specimen is heated to a target temperature T, temperature is maintained for exposure duration and then the load is increased till failure; (b) Unstressed test: Specimen is heated to a target temperature T. Temperature is maintained for exposure duration and then the specimen is tested under heated condition till failure; and (c) Residual property: Specimen is heated to a target temperature T. Temperature is maintained for exposure duration and then the specimen is cooled and tested till failure.

75% at 600 °C [15]. A review of the state-of-the-art on fire performance of HSC [26,27] identified two main differences between HSC and NSC at elevated temperature: (1) the difference in heat-induced relative strength loss in the intermediate temperature range (100 °C–400 °C) and (2) the occurrence of explosive spalling failure in HSC specimens at similar temperatures (200 °C–400 °C). The higher susceptibility of HSC to explosive spalling is due, in part, to its lower permeability, which limits the ability of water vapor to escape from the pores. This results in a build-up of pore pressure within the cement paste. As heating increases, the pore pressure also increases. This increase in vapor pressure continues until the internal stresses become so large to result in sudden, explosive spalling. Given the potential benefits of HSC and its increased usage, questions about its fire performance need to be resolved. In addition, the applicability of existing fire-design provisions, which were developed mostly from the results of fire tests on NSC, to HSC needs to be evaluated.

Many models are available in the literature for predicting the residual strength of concrete after high temperature exposure [4–6,28–33]. However, these existing models either deal mostly with NSC or were developed from very limited number of experimental data on HSC that was not large enough to cover a wide range of different variables and their combinations. This work aims to develop predictive relationships between the most affecting parameters and the resulting loss in the compressive strength of concrete for use in structural fire design. The heterogeneous nature of concrete leads to significant variability in its properties, making a deterministic prediction of its behavior difficult. This has led to the bulk of the previous research on the temperature-dependent properties of concrete being experimental. As a result, a theoretical development is not sought in this study, and the proposed models will be based on a statistical analysis of the existing test data from previous research.

Aslani and Bastami [30] proposed constitutive relationships for NSC and HSC exposed to fire to provide efficient modeling and specify the fire-performance criteria for concrete structures exposed to fire. These relationships were developed for unconfined NSC and HSC specimens that include compressive and tensile strengths, compressive elastic modulus, and compressive and tensile stress-strain relationships at elevated temperatures. The proposed relationships at elevated temperatures were compared with the experimental results and previous existing relationships revealing several advantages and disadvantages of present stress-strain relationships. These results were used to establish more accurate and general compressive and tensile stress-strain relationships. However, the experimental database used to develop the relationships for HSC is not only very limited (less than 100 specimens were used) but only covers siliceous aggregate concrete. Authors recommended adding more experimental results to the data to cover a broader range of different variables and their combinations.

The intricate nature of relationships among the variables for predicting the residual strength of HSC after the exposure to elevated temperature is a great hindrance for the development of regression-based models. Moreover, the database of available experiments being noisy, the adoption of regression models may not be a good choice. The neural network predictions have been found to greatly improve the predictions of complex phenomena involved in different disciplines of engineering including civil engineering problems [34–38]. This is mainly evident from the employment of many effective features including useful automatic search algorithms and adaptation capability for simulating the multivariate relationships among the causative factors. However, the use of artificial neural network (ANN) requires a sufficiently huge data set to cover the possible ranges of various causative factors and their combinations. Both dimensioned and dimensionless variables with the network having a single as well as two hidden layers were successfully used in the above cited studies [34–38] for predicting the output with the help of ANN models. Although single hidden layer was found enough for the ANN models in most of the studies [34,36–38], two hidden layers were recommended to be used for predicting the residual strength of non-linear ultrasonically evaluated damaged concrete [35], which may have been due to relatively less amount of data used in this study. It was reported that the increase in the number of neurons in a layer increases the prediction capability of the network in the beginning, which subsequently becomes stationary.

Research conducted since the 1950s has resulted in a considerable amount of data on the behavior and properties of HSC under elevated temperatures. However, a comprehensive evaluation of this data is lacking. The concrete strength models proposed in this study aim to fill this gap by using a large data set to increase statistical robustness. This research employs a large test set obtained from the survey of available

Table 1
Models for residual compressive strength of concrete after high temperature exposure.

Code/Researcher	Compressive strength after high temperature exposure
Eurocode 2: EN 1992-1-2 (2004)	Table 3.1 of the code For $41.4 < f'_{c,R} < 55.0$ MPa Table 6.1 N of the code For $f'_{c,R} \geq 55$ MPa
ACI 216.1–07 (2007)	Fig. 2.12(a) of the code For siliceous aggregates Fig. 2.12(b) of the code For calcareous (carbonate) aggregate
ASCE Manual (1992)	$R = 1$ For $20\,^{\circ}C \leq T \leq 450\,^{\circ}C$ $R = p + q\,T$ For $450\,^{\circ}C \leq T \leq 874\,^{\circ}C$ ($p = 2.05806$, $q = -0.002353$) $R = 0$ For $T > 874\,^{\circ}C$
Kodur et al. (2004)	$R = p + q\,T$ For $20\,^{\circ}C \leq T \leq 100\,^{\circ}C$ ($p = 1.0625$, $q = 0.0625$) $R = 0.75$ For $100\,^{\circ}C \leq T \leq 400\,^{\circ}C$ $R = p + q\,T$ For $T > 400\,^{\circ}C$ ($p = 1.33$, $q =$ -0.00145)
Nielsen et al. (2004)	$R = p + q\,T + s\,T^2$ For $20\,^{\circ}C \leq T \leq 810\,^{\circ}C$ ($p = 0.99936$, $q = 6.4 \times 10^{-5}$, $s = -1.6 \times 10^{-6}$)
Aslani and Bastami (2011)	For siliceous aggregates and $41.4 < f'_{c,R} < 55.2$ MPa: $R = p + q\,T$ For $20\,^{\circ}C \leq T \leq 100\,^{\circ}C$ ($p = 1.012$, $q = -0.0005$) $R = p + q\,T + s\,T^2 + u\,T^3$ For $100\,^{\circ}C \leq T \leq 800\,^{\circ}C$ ($p = 0.985$, $q = 0.0002$, $s = -2.235 \times 10^{-6}$, $u = 8.0 \times 10^{-10}$) $R = p + q\,T$ For $800\,^{\circ}C \leq T \leq 1000\,^{\circ}C$ ($p = 0.44$, $q = -0.0004$) $R = 0$ For $T > 1000\,^{\circ}C$ For siliceous aggregates and $55.2 \leq f'_{c,R} \leq 80$ MPa: $R = p + q\,T$ For $20\,^{\circ}C \leq T \leq 200\,^{\circ}C$ ($p = 1.01$, $q = -0.00068$) $R = p + q\,T + s\,T^2 + u\,T^3$ For $200\,^{\circ}C \leq T \leq 400\,^{\circ}C$ ($p = 0.935$, $q = 0.00026$, $s = -2.13 \times 10^{-6}$, $u = 8 \times 10^{-10}$) $R = p + q\,T + s\,T^2 + u\,T^3$ For $400\,^{\circ}C \leq T \leq 800\,^{\circ}C$ ($p = 0.9$, $q = 0.0002$, $s = -2.13 \times 10^{-6}$, $u = 8 \times 10^{-10}$) $R = p + q\,T$ For $800\,^{\circ}C \leq T \leq 1000\,^{\circ}C$ ($p = 0.44$, $q = -0.0004$) $R = 0$ For $T > 1000\,^{\circ}C$ For siliceous aggregates and $f'_{c,R} > 80$ MPa: $R = p + q\,T$ For $20\,^{\circ}C \leq T \leq 500\,^{\circ}C$ ($p = 0.8$, $q = -0.0005$) $R = p + q\,T + s\,T^2 + u\,T^3$ For $500\,^{\circ}C \leq T \leq 800\,^{\circ}C$ ($p = 0.96$, $q = -0.0008$, $s = -5.17 \times 10^{-7}$, $u = 4 \times 10^{-10}$) $R = p + q\,T$ For $800\,^{\circ}C \leq T \leq 1000\,^{\circ}C$ ($p = 0.44$, $q = -0.0004$) $R = 0$ For $T > 1000\,^{\circ}C$ For calcareous aggregates: $R = p + q\,T$ For $20\,^{\circ}C \leq T \leq 200\,^{\circ}C$ ($p = 1.01$, $q = -0.0006$) $R = p + q\,T + s\,T^2 + u\,T^3$ For $200\,^{\circ}C \leq T \leq 900\,^{\circ}C$ ($p = 1.0565$, $q = 0.0017$, $s = 5 \times 10^{-6}$, $u = -5 \times 10^{-9}$) $R = 0$ For $T > 900\,^{\circ}C$
Choe et al. (2015)	$R = 1$ For $T \leq 20\,^{\circ}C$ $R = p + q\,T$ For $20\,^{\circ}C < T \leq 100\,^{\circ}C$ ($p = 1.0375$, $q =$ -0.0019) $R = 0.85$ For $100\,^{\circ}C < T \leq 200\,^{\circ}C$ $R = p + q\,T$ For $200\,^{\circ}C < T \leq 700\,^{\circ}C$ ($p = 1.1$, $q =$ -0.0013) $R = p + q\,T$ For $700\,^{\circ}C < T \leq 900\,^{\circ}C$ ($p = 0.62$, $q =$ -0.0006) $R = p + q\,T$ For $900\,^{\circ}C < T \leq 1200\,^{\circ}C$ ($p = 0.32$, $q =$ -0.0003) $R = 0$ For $T > 1200\,^{\circ}C$
Phan and Carino (2003)	$R = 1$ For $T \leq 50\,^{\circ}C$ $R = p + q\,T$ For $50\,^{\circ}C < T \leq 100\,^{\circ}C$ ($p = 1.28$, $q =$ -0.0056) $R = 0.72$ For $100\,^{\circ}C < T \leq 350\,^{\circ}C$ $R = p + q\,T$ For $350\,^{\circ}C < T \leq 778\,^{\circ}C$ ($p = 1.31$, $q =$ -0.00168) $R = 0$ For $T > 778\,^{\circ}C$
Hertz (2005)	$\frac{1}{R} = 1 + \frac{T}{1000} + \left(\frac{T}{780}\right)^2 + \left(\frac{T}{490}\right)^8 + \left(\frac{T}{100000}\right)^{64}$

T = elevated temperature in °C; R = ratio of residual compressive strength to the compressive strength of concrete at room temperature; $f'_{c,R}$ = compressive strength of concrete at room temperature; p, q, s, and u = model parameters.

test results on HSC after high temperature exposure. The data was carefully analyzed statistically to ascertain the impact of different independent variables on the unstressed residual strength of HSC. The compiled test data was compared with existing design models from codes, standards, guidelines, and researchers. Finally, new ANN based models were proposed for predicting the residual strength of HSC after high temperature exposure. The predicted values of the residual concrete strength were then compared with those predicted by the available models. For predicting the design values of the residual strength of HSC, new ANN models were also proposed. The proposed design models are recommended for use in structural fire design.

2. Available design models

The models, available in the literature for predicting the residual compressive strength of concrete after high temperature exposure, are listed in Table 1. The models are taken from three codes namely ACI 216.1–07 [5], ASCE Manual [6], and Eurocode 2: EN 1992-1-2 [4]. Table 1 also lists the models proposed by researchers such as Aslani and Bastami [30], Choe et al. [31], Hertz [33], Kodur et al. [28], Nielsen et al. [29], and Phan and Carino [32] and for the prediction of residual compressive strength of concrete. The salient features of the available models listed in Table 1 are discussed in subsequent subsections.

2.1. Effect of aggregate type

For NSC, the siliceous aggregate has better fire resistance (unstressed residual) as compared to the calcareous aggregates [5]. For HSC, only Aslani and Bastami [30] make a distinction between the type of aggregates. Whereas, the effect of aggregate type on HSC is not clearly established in other models:

i) ACI 216.1–07 [5] curves are plotted only for NSC. Therefore, the effect of aggregate type on the residual strength of HSC is not known, but the code does not provide any limit on the compressive strength of concrete for the applicability of these curves.

ii) ASCE Manual [6] uses the ACI 216.1–07 [5] curves but proposes a simplified linear model for predicting the residual compressive strength of concrete irrespective of the type of aggregates.
iii) Eurocode 2: EN 1992-1-2 [4] considers the effect of aggregate type (siliceous or calcareous) for concrete of $f'_{c,R} < 55.0$ MPa, but it is not considered for high strength concrete with $f'_{c,R} \geq 55.0$ MPa.

2.2. Effect of test methods

As per ACI 216.1–07 [5], among the three types of test methods shown in Fig. 1, the unstressed residual property tests give the lowest residual strength of concrete. Thus this test method, usually employed in experiments due to the requirement of the least efforts, is the most conservative. Other models do not show the effect of different test methods.

2.3. Limits of applicability

ACI 216.1–07 [5] and ASCE Manual [6] make no distinction between the normal and high strength concrete due to which there is no limit imposed on the compressive strength of concrete for using the curves plotted for normal strength concrete. From the typical values for which plots are given, it appears that the models of the two codes are only meant for normal strength concrete. The maximum temperature covered in these figures is up to 871 °C (i.e., 1600 °F).

The residual strength model of Eurocode 2: EN 1992-1-2 [4] is not applicable for concrete strength greater than 90 MPa.

2.4. Level of complexity

Most of the code models are either based on the use of graphs or simplified model. On the other hand, the models proposed by Kodur et al. [28], Choe et al. [31] and Phan and Carino [32] are piecewise linear for different temperature ranges. However, Choe et al. [31] used a maximum of seven temperature ranges thus giving five equations for predicting the residual compressive strength of concrete.

It is only the models of Nielsen et al. [29] and Hertz [33], which provide single equation for whole range of T. The model of Nielsen et al. [29] is quadratic in T. Whereas, Hertz [33] used a complicated rational function with numerator as unity and the denominator as a 64-degree polynomial of T.

Aslani and Bastami [30] developed equations to predict the residual compressive strength of concrete for different ranges of f'_c and temperature. The proposed equations are either linear or cubic in T.

3. Database used in the study

The experimental data on the residual strength of HSC after exposure to elevated temperature was collected from accessible literature such as technical reports, master and Ph.D. theses, journal papers and conference proceedings. The database covered a wide range of various variables and their combinations affecting the residual concrete strength. The selection of data was dome judiciously and only the experiments providing most material and geometric characteristics were used. The database contains results of 460 specimens. The whole database covered 54 experimental studies conducted during the period from 1965 to 2017 [7,10,11,23,39–50,51-88]. The criteria adopted for the selection of data were:

i) Data is for plain concrete cylinders, cubes, and stub columns tested in compression.
ii) Data covers only the high strength concrete specimens with specified concrete strength exceeding 41.4 MPa, as per the limit set by the ACI 363R-10 [2].
iii) Ordinary Portland cement was used in all concrete mixes containing no fibers. Mineral additives in the concrete mix such as silica fume or fly ash do not exceed 15% of the cement by weight.
iv) The test specimens are exposed to elevated temperature and the temperature is then held constant to achieve the steady state condition. The specimens are then cooled down naturally (air cooling) to the room temperature. Subsequently, specimens are tested under axial compression until failure to measure their residual strength.
v) Sufficient details are provided about different material characteristics and geometry of specimens to enable the use of the results with confidence.
vi) The data covers 177 data points (38.5%) for calcareous aggregates, 228 for siliceous aggregates (49.6%), and the aggregate type of the remaining 55 (11.9%) is either not known or is silico-calcareous.

As the database is for cube and cylinder specimens of different dimensions, the conversion factors, proposed by Yi et al. [89], were used to obtain the specified compressive strength of the standard 150 × 300 mm concrete cylinder.

4. Data analysis

The data was analyzed statistically to calculate quartiles, mean, standard deviation (SD), coefficient of variation (CV), skewness, kurtosis, and Anderson Darling normality test. The values of these statistical parameters are given in Table 2. The skewness was calculated to check asymmetry in the distribution of the data. The positive skew indicates that the data has a long tail in the positive direction and skewness greater than 1 means highly skewed data. The kurtosis of the data, given in Table 2, was calculated to ascertain the shape of data distribution. For the data to follow the normal distribution, kurtosis should be 3. Marginal plots for different pair of variables namely $f_{c,R}$ vs

Table 2
Statistics of input parameters (460 data points).

Statistical parameter	Aggregate/binder ratio	Water/binder ratio	Soaking period, h (h)	Heating rate, H_r (°C/min)	Elevated Temp., T (°C)	$f'_{c,R}$ (MPa)
Minimum (Q0)	0.822	0.13	0.5	0.500	50	41.466
First quartile (Q1)	1.940	0.29	1.0	2.500	250	48.442
Second quartile (Q2, median)	2.268	0.32	2.0	4.000	400	66.740
Third quartile (Q3)	2.761	0.45	3.0	8.083	600	82.406
Fourth quartile (Q4, Maximum)	4.588	0.60	11.5	20.000	1200	140.551
Mean	2.293	0.358	2.177	5.973	481.587	67.809
Standard deviation	0.645	0.109	1.786	5.795	263.877	19.757
Coefficient of variation (%)	28.15	30.42	82.04	97.01	54.79	29.14
Skewness	0.232	0.628	2.484	1.446	0.511	0.609
Kurtosis	−0.042	−0.443	7.545	1.037	−0.295	0.243
Anderson Darling normality test						
A-Squared	1.99	11.27	45.63	37.01	7.26	6.33
P-Value	< 0.005	< 0.005	< 0.005	< 0.005	< 0.005	< 0.005

$f'_{c,R}$ = compressive strength of concrete at room temperature.

w/b; H_r vs t_s; $f_{c,T}/f_{c,R}$ vs a/b; and $f_{c,T}/f_{c,R}$ vs T; are plotted in Figs. 2–5 respectively. The pairs are selected for minimizing the duplication and for getting better insight into the data. The observations made from the statistical analysis and the marginal plots are:

i) The large values of SD and CV (28.2%–99.4%) for all variables show that the data is spread on a wide range.
ii) The P-values for all variables are less than 0.005 which means that the null hypothesis (that the distribution is normal) is rejected and thus the distribution is not normal. The A-squared value of all variables is greater than 1.159 (at 0.5% significance level) which further confirms the non-normality of data distribution.
iii) Generally, the reduction in w/b ratio resulted in an increase in the compressive strength of concrete at room temperature (Fig. 2). However, there are some exceptions which may be due to several factors such as the level of compaction, quantity and type of superplasticizer, type of mineral admixtures, etc.
iv) Although a wide range of compressive strength of concrete is covered starting from the lower limit of high strength concrete and covers even the ultra-high strength concrete (41.5–140.6 MPa), the data for the ultra-high strength concrete is quite low with only 6.2% data for strength greater than 100 MPa. Most of the data of compressive strength is in the lower range (Fig. 2) with 27.2% data for strength less than 50 MPa thus having a positive tail (Fig. 2) which is also reflected in positive skewness of 0.609 (Table 2).
v) The water to binder ratio shows large variation, varying from 0.13 to 0.6 (Fig. 2 and Table 2), because of the use of mixes prepared with or without the use of superplasticizers for achieving a wide range of compressive strengths of concrete. Maximum data is for w/b ratio close to 0.3 (Fig. 2) which is close to the median (i.e. 0.32 (Table 2). The w/b data also has a longer positive tail (Fig. 2)

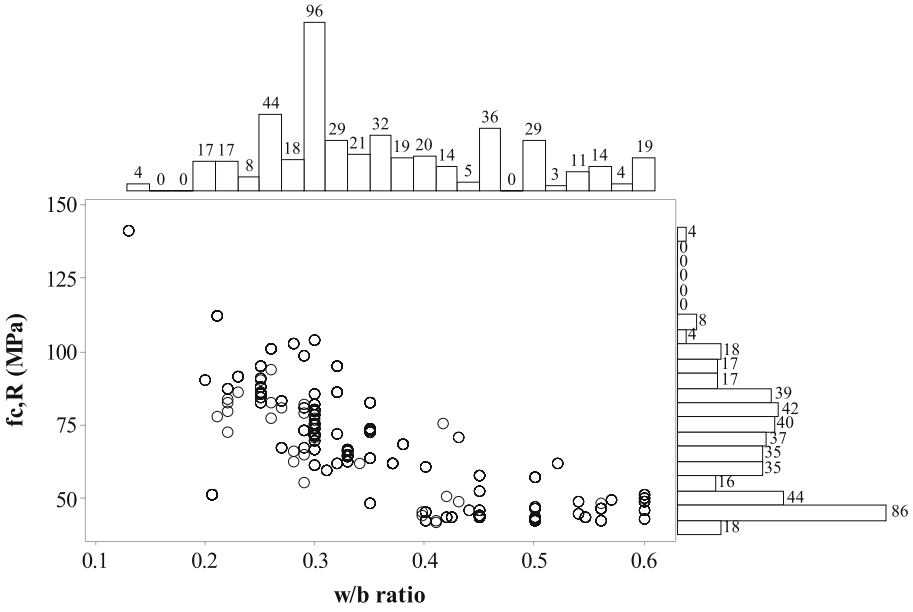

Fig. 2. Marginal plot of fc,R vs w/b ratio.

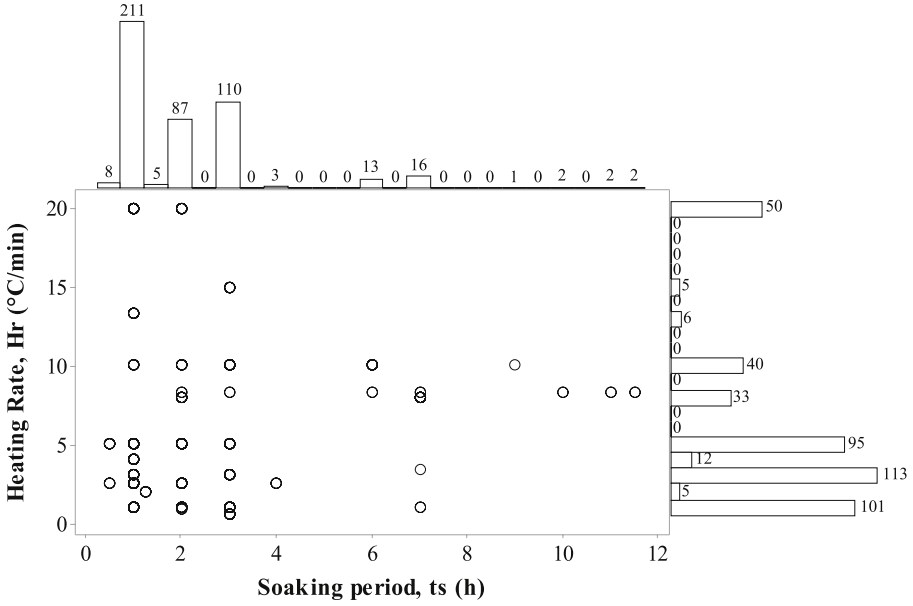

Fig. 3. Marginal plot of heating rate, Hr vs soaking period, ts.

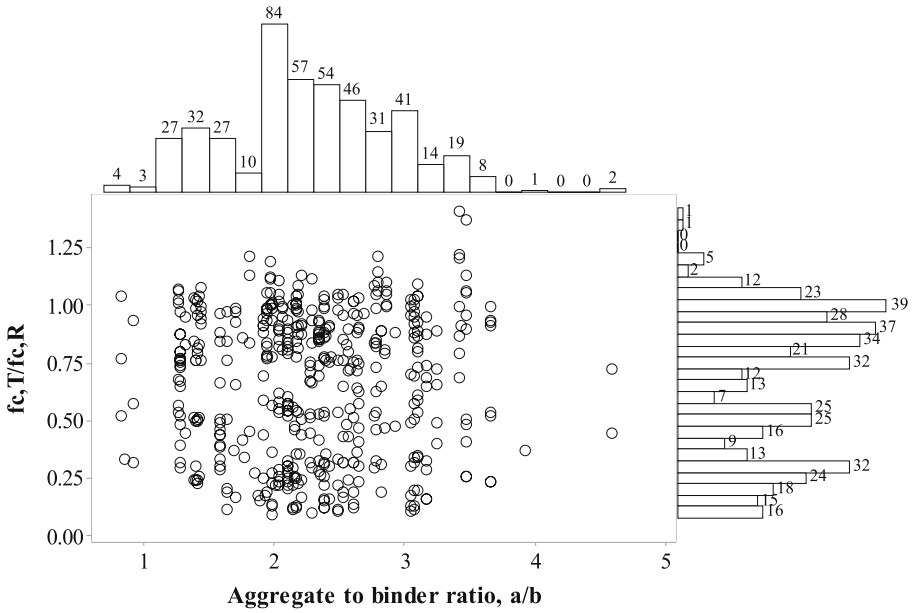

Fig. 4. Marginal plot of fc,T/fc,R vs aggregate to binder ratio, a/b.

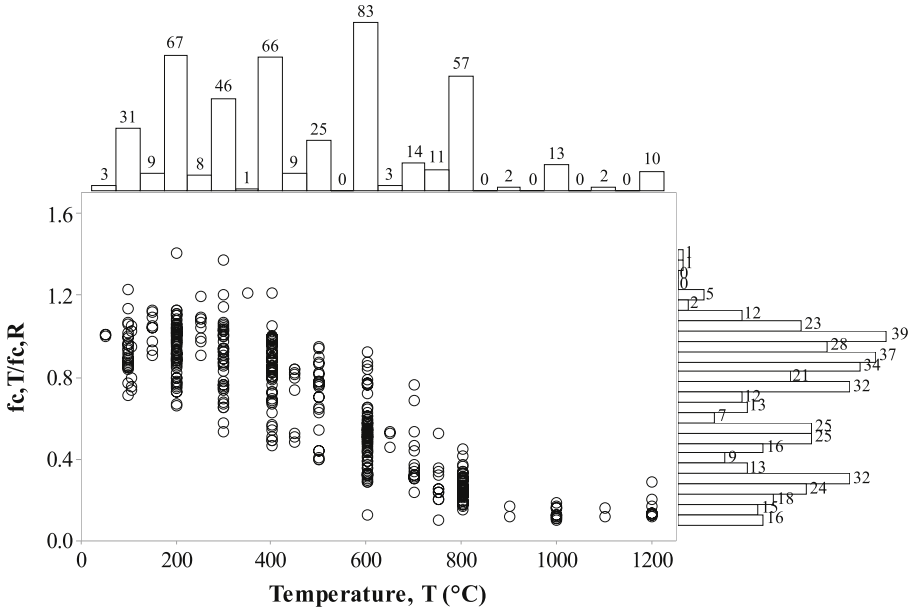

Fig. 5. Marginal plot of $f_{c,T}/f_{c,R}$ vs T.

and thus the distribution is skewed with a skewness of 0.628 (Table 3).

vi) Although the soaking period, h, varies from 0.5 to 11.5 h, most of the data (about 90%) varies from 1 to 3 h (Fig. 3) with maximum data (45.9%) having 1 h soaking period. Thus only little data (8.5%) is for t_s more than 3 h. This shows that the data is heavily skewed with a skewness of 2.484 indicating a long positive tail. In addition, because of the sharp peak, kurtosis is also very high (7.545, as shown in Table 2). Moreover, the A-squared of Anderson Darling normality test is also very high (45.63, as shown in Table 2), which indicates large deviation from the normal distribution.

vii) Although the heating rate varies from 0.5 to 20 °C/min, the peak rate is much lower than that is attained in standard fire [90–92]. However, the peak temperature of many experiments reaches up to 1200 °C, which corresponds to the peak fire temperature. The

Table 3
Pearson r for correlation between different variables and the residual compressive strength of concrete.

Variable	Pearson r	P-Value	Remark
a/b	0.023	0.625	No correlation
w/b	0.084	0.072	Positive weak and less significant correlation
h	0.270	0.000	Positive weak and significant correlation
H_r	−0.060	0.196	No correlation
T	−0.870	0.000	Negative strong and significant correlation
$f'_{c,R}$	−0.102	0.028	Negative weak and significant correlation

a/b = aggregate to binder ratio; w/b = water to binder ratio; h = soaking period; H_r = heating rate; T = elevated temperature; $f'_{c,R}$ = compressive strength of concrete at room temperature.

distribution of data is erratic (Fig. 3) with most of the data (about 70.9%) for $H_r \leq 5$ °C/min and some of the data (15.9%) is in the range of 5–10 °C/min. Moreover, there is 10.9% data having $H_r = 20$ °C/min. Thus the data is highly skewed with a skewness of 1.446 (Table 2). The A-squared of Anderson Darling normality test is also quite high (37.01, as shown in Table 2) showing non-normal distribution.

viii) It is observed from the table that the data covers a wide range of aggregate to binder ratio, *a/b*, which varies from 0.82 to 4.59 (Fig. 4). The distribution is much better than other variables due to which the skewness is minimum (0.232, as given in Table 2) and A-squared of Anderson Darling normality test is also not very high (1.99, as shown in Table 2). However, the data is not following the normal distribution. The scatter of the data shown in Fig. 4 does not apparently show any correlation with the residual strength of concrete.

ix) Fig. 5 shows the marginal plot of the residual strength of concrete vs elevated temperature, *T*. The elevated temperature varies from the extreme hot weather temperature of 50 °C to the fire temperature of 1200 °C. However, the peak heating rate of 20 °C/min is much lower than that attained in standard fire [90–92]. The values of skewness, kurtosis and Anderson Darling normality test reported in Table 2 show that the data is not following the normal distribution. The data is positively skewed with a longer positive peak (skewness = 0.511) and flatter peak as compared to the normal (kurtosis = −0.295). The scatter plot shows that with the increase in the elevated temperature, there is initial small increase in strength of concrete which reduces subsequently and almost loses its strength at about 1200 °C. Some very low values of residual strength at relatively low temperature may be due to the adverse effects of different types of superplasticizers used in concrete mixes. Fig. 6 provides the detailed statistical plots of elevated temperature, *T*, which is the most significant variable. The figure covers frequency histogram, frequency polygon, interquartile ranges, and 95% confidence intervals for mean and median.

x) Although some of the experiments show an increase in compressive strength of concrete after exposure to a relatively low temperature, none of the available models show this trend. As this is not a consistent trend, it was ignored in the available models and also in our proposed ANN models. Most of the models show a decrease in the compressive strength of concrete for temperature greater than 20 °C or 50 °C [32]. However, ASCE Manual [6] shows no effect of temperature up to 450 °C.

Besides the above parameters, there are some other parameters such as the type and quantity of superplasticizer, moisture content at the time of testing the specimen, that may also affect the residual compressive strength of HSC. But because of the non-availability of their values, these variables are ignored in this study. These variables are also ignored in the available models (Table 1).

Besides providing an understanding of the data and its distribution, the above analysis will be helpful for researchers in designing future experiments for data augmentation.

5. ANN models

ANN based models have been described by several researchers in detail [e.g. 34–38]. The basic concept of ANN modeling is based on

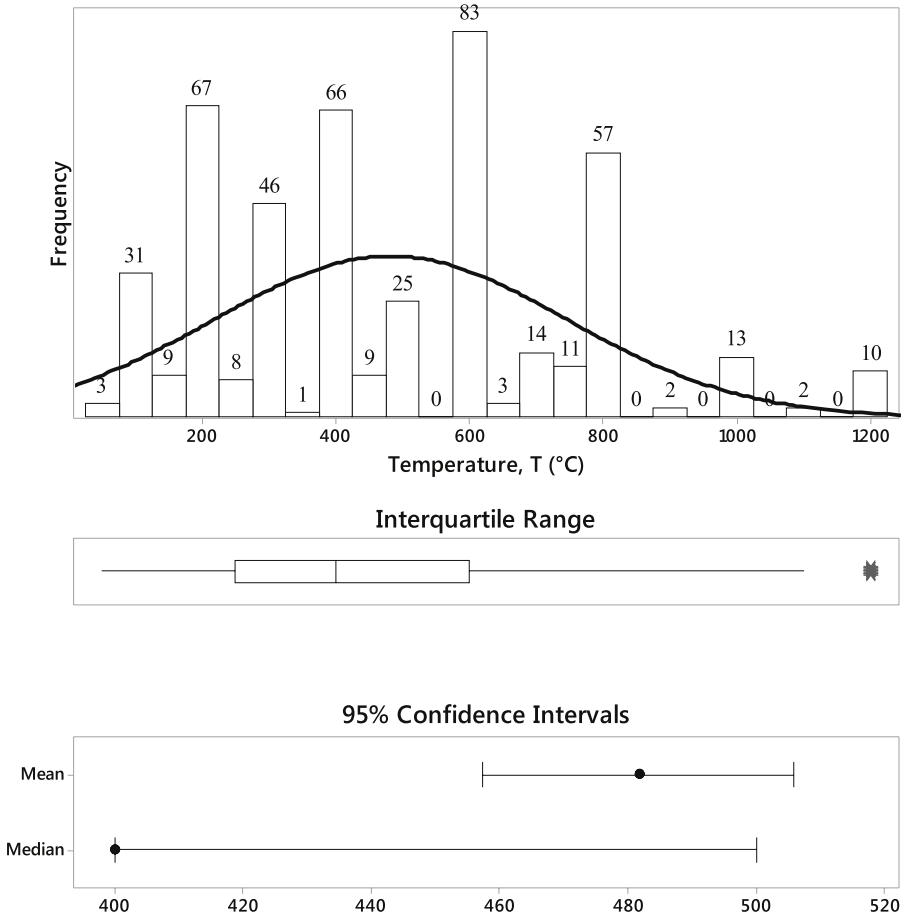

Fig. 6. Statistical analysis of elevated temperature, *T*.

establishing the relationship between the data of independent and dependent variables by employing training methods [36–38]. The ANN model used for developing a causal relationship between the residual concrete strength and independent variables, employs the input namely, coarse aggregate type, aggregate to binder ratio, a/b, water to binder ratio, w/b, soaking period in hour, h, heating rate in °C/min, H_r, exposure temperature in °C, T, compressive strength of concrete at ambient temperature in MPa, $f'_{c,R}$, and yields the output, which is the ratio of residual compressive strength of concrete after exposure to temperature T, $f'_{c,T}$, to $f'_{c,R}$. The data was segregated based on the aggregate types. Out of the total 460 data sets, there were 177 data sets for calcareous aggregates, 228 data sets for siliceous aggregates, and the aggregate type of the remaining is either not known or is silico-calcareous. The models ANN1 and ANN2 were developed for calcareous and siliceous aggregates and these models employed 177 and 228 data sets respectively. Another model ANN3 was developed for the total data set so as to investigate the error introduced in the model when aggregate type is ignored. The three models used in the study are as under:

$$\text{Model} - \text{ANN1: } \frac{f'_{c,T}}{f'_{c,R}} = g_1(a/b,\ w/b,\ h,\ H_r,\ T,\ f'_{c,R}) \text{for calcareous aggregates} \quad (1)$$

$$\text{Model} - \text{ANN2: } \frac{f'_{c,T}}{f'_{c,R}} = g_2(a/b,\ w/b,\ h,\ H_r,\ T,\ f'_{c,R}) \text{ for siliceous aggregates} \quad (2)$$

$$\text{Model} - \text{ANN3: } \frac{f'_{c,T}}{f'_{c,R}} = g_3(a/b,\ w/b,\ h,\ H_r,\ T,\ f'_{c,R}) \text{for all types of aggregates} \quad (3)$$

As there is no ideal distribution of the data between training and validation/testing, the training of the neural network in this study was performed using two-third of the data [34–38]. Thus 118, 152, and 307 data sets were used for the training of models ANN1, ANN2 and ANN3 respectively. The selection of the data set for training purposes was done randomly. The testing and validation of the networks of the models were performed using the remaining one-third of the data (i.e. 59, 76, and 153 for the three models respectively), which was not used in the development of the models.

The neural network architecture of the three models (Eq. (1) to (3)), is presented in Fig. 7 for the training scheme. The neural network architecture of the models employs a single hidden layer. In Fig. 7, n1 is the number of independent variables involved in the model and n2 is the number of neurons in the hidden layer. The value of n2 for the sensitivity analysis (i.e. for Models ANN1, ANN2, and ANN3) was taken as 12. However, the value of n2 for the final proposed models (i.e. Models ANN1, ANN2, and ANN3) was optimized by varying it from 9 to 12. The results reported in the paper were obtained after 100 runs of ANN for each case. Besides passing the input through the hidden layer, it was also passed directly to the output layer, as shown in Fig. 7.

5.1. Neural network training

The training of the network consists of optimizing the parameters viz. weights and biases in order to minimize an error function computed from predicted and target data. Three neuron models namely, tansig, logsig, and purelin, were used in the architecture of the network with the back propagation algorithm. In the back propagation algorithm, the feed-forward (FFBP), cascade-forward (CFBP) and Elman back propagation (EBP) type networks were considered. Levenberg-Marquardt nonlinear least square fitting method (1963) was employed for training the networks. Each input is weighted with an appropriate weight and the sum of the weighted inputs and the bias forms the input to the transfer function. The neurons employed the following differentiable transfer function to generate their output:

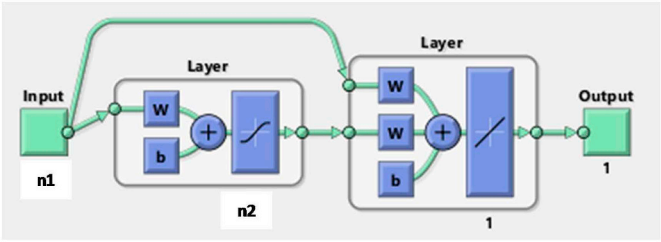

Fig. 7. Neural network models with one hidden layer (w is the weight and b is the bias; For Model-ANN1, Model-ANN2, and Model-ANN3: n1 = 6 and n2 = 12; For Model-ANN1-R: n1 = 2 and n2 = 9 to 12; For Model-ANN2-R and Model-ANN3-R: n1 = 3 and n2 = 9 to 12).

$$y_j = f_1(z_j) = \left(1 + e^{-z_j}\right)^{-1} \text{for log} - \text{sigmoid transfer function} \quad (4)$$

$$y_j = f_2(z_j) = 2\left(1 + e^{-2z_j}\right)^{-1} - 1 \text{ for tan} - \text{sigmoid transfer function} \quad (5)$$

$$y_j = f_3(z_j) = z_j \text{ for linear transfer function} \quad (6)$$

where,

$$z_j = \sum_i W_{ij} x_i + b_j \quad (7)$$

The weight, W, and biases, b, of these equations are determined in such a way as to minimize the energy function. The sigmoid transfer functions generate output between 0 and 1 or -1 and +1 as the neuron's net input goes from negative to positive infinity depending upon the use of log or tan sigmoid. When the last layer of a multilayer network has sigmoid neurons (log or tan) then the output of the network is limited to a small range (0–1 for log-sigmoid and −1 to 1 for tan-sigmoid), whereas, the output of linear output neurons can take on any value varying from $-\infty$ to $+\infty$ [93].

The preprocessing of the network training set was performed by normalizing the inputs and targets so that their mean is zero and standard deviations as unity. Similarly, all weights and bias values were initialized to random numbers. While the numbers of input and output nodes are fixed, the hidden nodes in the case of FFBP were subjected to trials and the one producing the most accurate results was selected. The performance of all neural network model configurations was based on the mean percent error (MPE), mean absolute percent error (MAPE), root mean square error (RMSE), and coefficient of determination, R^2, of the linear regression line between the predicted values from the neural network model and the desired outputs. CFBP is similar to FFBP, but it includes a connection from the input and all previous layers to the following layers. The input is directly connected to the output and the values obtained from the hidden layers and the input layers are compared and weights are adjusted accordingly. The training of these networks was stopped after reaching the minimum mean square error between the network yield and true output over all the training patterns or when the number of iterations exceeded a prescribed maximum. The process was repeated several times for obtaining the optimal neural network model configuration.

6. Sensitivity analysis

The sensitivity of different causative factors was investigated using the ANN as well as the statistical methods such as Pearson correlation coefficient (or Pearson's r) and Spearman's rank correlation coefficient (or Spearman's rho).

6.1. Statistical methods

Table 3 shows the Pearson's r values and the corresponding P-values for a linear correlation between different variables and the residual strength of concrete after exposure to elevated temperature. The Pearson's r values vary from −1 to +1. The extreme values of −1 and +1 show strong negative and positive correlations respectively, whereas zero value indicates no correlation. A positive correlation

indicates that an increase in the value of a variable has a positive effect on the dependent variable i.e. causes an increase in the residual compressive strength of concrete, which is the dependent variable. The P-value is the probability that the null hypothesis of no correlation is valid. A small P-value (≤ 0.05) provides strong evidence for rejecting the null hypothesis, whereas a large P-value, we fail to reject the null hypothesis. The values reported in the table show that the variables a/b and H_r have no correlation, whereas the exposure temperature, T, is the only variable that has a strong and significant correlation. The correlation for f_c' is negative weak but significant. Although the soaking period, h, has a significant positive correlation, but logically the variable h cannot have a positive correlation and thus the soaking period data was ignored for being doubtful. The linear correlation for the remaining variables is either weak or less significant. The probability of accepting the null hypothesis (i.e. no correlation) for the water to binder ratio, w/b, is 7.2%. Thus, if the significance level is raised from 5% to 10%, w/b also has less a significant, positive but weak correlation.

Pearson's correlation requires that the variables follow the normal distribution and are equally distributed about a linear regression line. However, the normality requirement is only an exhaustive measure of association if the joint distribution is bivariate normal [94]. As these conditions may not be applicable to the data used in the analysis, the correlation between different variables and the residual strength of concrete after exposure to elevated temperature was also assessed using Spearman rho values presented in Table 4. In line with the three ANN models, the Spearman rho values are also calculated for the three groups of the data i.e. two types of aggregates (calcareous and siliceous) and all aggregate types. It is to be noted here that like Pearson's r values, the Spearman rho also varies from -1 to 1. The positive rho values indicate positive correlation i.e. an increase in the value of the variable increases the residual strength, whereas the negative values indicate negative correlation. The corresponding P-values are also given in the table. The variables showing statistically significant correlation are written in bold. Obviously, T is the most significant variable showing a strong negative correlation for all the three groups of data. For all data, after ignoring the soaking period, h, as discussed above, the variables having correlation in order of decreasing sensitivity are: T, w/b, and f_c'. For calcareous aggregates, T is the lone variable showing correlation, whereas for siliceous aggregates, the variables showing a correlation in order of decreasing sensitivity are: T, a/b, and w/b. One interesting observation from the Spearman rho values for the data of siliceous aggregates is that the aggregate to binder ratio shows positive weak and significant correlation indicating that the increase in the aggregate to binder ratio causes increase in the residual compressive strength of concrete. This shows that the siliceous aggregates help in resisting fire, which is in line with the findings of earlier researchers.

Table 4
Spearman rho for correlation between different variables and the residual compressive strength of concrete.

Variable	Spearman rho	P-Value	Remark
Calcareous aggregates			
a/b	0.050	0.509	No correlation
w/b	0.078	0.305	No correlation
h	0.064	0.398	No correlation
H_r	−0.074	0.328	No correlation
T	−0.782	0.000	**Negative strong and significant correlation**
$f'_{c,R}$	−0.005	0.948	No correlation
Siliceous aggregates			
a/b	0.142	0.032	**Positive weak and significant correlation**
w/b	0.124	0.061	Positive weak and less significant correlation
h	0.102	0.125	No correlation
H_r	0.034	0.607	No correlation
T	−0.942	0.000	**Negative strong and significant correlation**
$f'_{c,R}$	−0.088	0.183	No correlation
All types of aggregates			
a/b	0.020	0.670	No correlation
w/b	0.087	0.062	Positive weak and less significant correlation
h	0.242	0.000	**Positive weak and significant correlation**
H_r	0.037	0.433	No correlation
T	−0.857	0.000	**Negative strong and significant correlation**
$f'_{c,R}$	−0.122	0.009	Negative weak and less significant correlation

a/b = aggregate to binder ratio; w/b = water to binder ratio; h = soaking period; H_r = heating rate; T = elevated temperature; $f'_{c,R}$ = compressive strength of concrete at room temperature.

6.2. Analysis using ANN

The sensitivity analysis was also performed using ANN by eliminating each input neuron in turn from the three models (Eq. (1) to (3)). The effect of elimination of an input neuron on the prediction of residual compressive strength of concrete after high temperature exposure was evaluated in terms of MPE, MAPE, RMSE, and R^2 criteria. The desirable value of MPE is zero, whereas its positive and negative values show over- and under-estimation respectively. The best performance of a prediction model is indicated by MPE, MAPE, and RMSE approaching to zero and R^2 approaching to unity. Table 5 shows the results of sensitivity analysis for the three models given by Eqs. (1)–(3). The network architecture of the model assumed in the sensitivity analysis consisted of 12 neurons in the hidden layer for all the three models (i.e. ANN1, ANN2, and ANN3). The value of epochs was taken as 100 in the development of the three ANN models because fewer epochs were enough for training the networks.

The results in Table 5 indicate that for the prediction of residual compressive strength of concrete after high temperature exposure, obviously, T is the most significant variable for all the three models as its elimination reduces the value of R^2 most significantly. However, there is a slight difference in the order of sensitivity of other variables in the three models. After ignoring the soaking period, h, as discussed above, the variables in the order of decreasing level of sensitivity for the three models are:

T, w/b, H_r, $f_{c,R}$ and a/b for Model ANN1

T, w/b, a/b, $f_{c,R}$ and H_r for Model ANN2

T, H_r, w/b, $f_{c,R}$ and a/b for Model ANN3

It is observed that w/b is either the second or third most sensitive variable. Its elimination from the three models reduces R^2 from 0.949 to 0.918, 0.958 to 0.955, and 0.933 to 0.919 respectively. Although the statistical analysis shows no correlation for w/b in calcareous aggregates because of large P-value (Table 4), it has been retained in ANN1 because of the significant effect of its elimination in ANN sensitivity analysis. The compressive strength of concrete at room temperature, $f'_{c,R}$, is the second least sensitive variable in all the models. However, it is found to show a less significant correlation (Table 4) for all aggregates and thus it is retained only in ANN3. Although a/b is the least significant variable in ANN1 and ANN3, it is the third most sensitive variable in model ANN2 (siliceous aggregates), as its elimination reduces the value of R^2 from 0.958 to 0.955. A similar observation has already been made based on the Spearman's rho values, where a/b is found to show a significant correlation (Table 4). Thus a/b need to be retained only in model ANN2. The variable H_r is the second most sensitive variable ANN3 and third most sensitive in ANN1, whereas in ANN2 it is the least significant. As the statistical analysis shows no correlation for H_r in any of the three models because of large P-values (0.328–0.607, as shown in Table 4) it may be eliminated from all the models.

Table 5
Sensitivity analysis of different ANN models with feed-forward back propagation for different sets of input variables.

Input variables	MPE	MAPE	RMSE	R^2
Model-ANN1 (n2 = 12)				
All (Eq. (1))	0.75	7.5	0.06	0.951
No a/b	1.81	6.8	0.08	0.952
No w/b	2.85	9.3	0.08	0.918
No h	0.62	8.5	0.07	0.921
No H_r	0.39	8.7	0.07	0.928
No T	20.85	41.2	0.23	0.238
No f_c'	1.97	8.1	0.07	0.930
Only T	3.58	17.7	0.14	0.734
Only T and f_c'	5.26	15.9	0.12	0.786
Only T, f_c' and w/b	3.09	11.3	0.10	0.850
Model-ANN2 (n2 = 12)				
All (Eq. (2))	2.14	11.5	0.07	0.958
No a/b	1.32	12.2	0.07	0.955
No w/b	2.19	10.8	0.07	0.955
No h	0.73	10.9	0.07	0.956
No H_r	2.16	11.7	0.07	0.957
No T	24.68	47.2	0.23	0.487
No f_c'	2.43	11.5	0.07	0.957
Only T	3.80	14.6	0.09	0.924
Only T and f_c'	2.59	13.5	0.08	0.934
Only T, f_c' and w/b	1.91	12.0	0.07	0.951
Model-ANN3 (n2 = 12)				
All (Eq. (3))	3.23	12.4	0.08	0.933
No a/b	3.53	13.9	0.08	0.926
No w/b	2.22	13.4	0.09	0.919
No h	3.32	13.6	0.09	0.922
No H_r	2.20	14.0	0.09	0.909
No T	23.4	48.0	0.24	0.396
No f_c'	2.19	13.5	0.09	0.923
Only T	5.98	18.8	0.13	0.810
Only T and f_c'	4.14	18.5	0.13	0.836
Only T, f_c' and w/b	4.38	16.6	0.11	0.871

a/b = aggregate to binder ratio; w/b = water to binder ratio; h = soaking period; H_r = heating rate; T = elevated temperature; $f'_{c,R}$ = compressive strength of concrete at room temperature; MPE = mean percent error; MAPE = mean absolute percent error; RMSE = root mean square error; R^2 = coefficient of determination.

Most of the available regression models (Table 1) for the prediction of residual compressive strength only include T except Eurocode 2: EN 1992-1-2 [4] and Aslani and Bastami [30] wherein different models are proposed for different ranges of the compressive strength of concrete, $f'_{c,R}$. However, the effect of its elimination in ANN3 has negligible influence on error estimates with R^2 reducing from 0.933 to 0.923 and RMSE increasing from 0.08 to 0.09. The effect of retaining only T shows a large reduction in R^2 as it reduces from 0.933 to 0.810. Thus the development of a model based on T alone may not be justified, which is also supported by the statistical analysis of correlations.

6.3. Effect of aggregate type

It is widely reported that the change in concrete properties due to the exposure to elevated temperature depends on the type of coarse aggregate used. For normal weight concrete, the aggregates may be calcareous or siliceous. The calcareous aggregates are generally from sedimentary rocks, which may include limestone or dolomite, whereas, the siliceous aggregates may include granite and sandstone. The difference in the thermal expansion of the two types of aggregates is mainly responsible for the difference in the behavior of concrete exposed to elevated temperature. The thermal expansion of calcareous aggregates starts at a lower temperature due to the dissociation of dolomite as compared to the siliceous aggregates (NRC, Canada).

The effect of aggregate type can be ascertained from the ANN sensitivity analysis. The consideration of T alone in the models ANN1 and ANN2 for the two types of aggregates (calcareous and siliceous), shows considerably different values of error estimates. For ANN1 and ANN2 models, the values of R^2 are 0.734 and 0.924 respectively, whereas the RMSE for the two models are 0.14 and 0.09 respectively (Table 5). The statistical analysis also justifies the development of separate models for the two types of aggregates. The Spearman's rho values of T for calcareous and siliceous aggregates are −0.782 and −0.942 respectively (Table 4), which are significantly different. Thus ignoring the aggregate type in the development of combined model ANN3 may not be a good idea. However, besides the development of separate models for the two types of aggregates (ANN1 and ANN2), the combined model ANN3 is also retained for the data for which aggregate type is not known.

7. Revised ANN models

Based on the sensitivity analysis, the ANN models are revised by eliminating the variables which do not show a significant correlation, as discussed in the previous section. Thus the revised models are:

$$\text{Revised Model} - \text{ANN1} - \text{R:}\frac{f'_{c,T}}{f'_{c,R}} = g_4(w/b,\ T) \text{ for calcareous aggregates} \quad (8)$$

$$\text{Revised Model} - \text{ANN2} - \text{R:}\frac{f'_{c,T}}{f'_{c,R}} = g_5(a/b,\ w/b,\ T) \text{ for siliceous aggregates} \quad (9)$$

$$\text{Revised Model} - \text{ANN3} - \text{R:}\frac{f'_{c,T}}{f'_{c,R}} = g_6(w/b,\ T,\ f'_{c,R}) \text{ for all types of aggregates} \quad (10)$$

The network architecture of the above models is shown in Fig. 7 for the back propagation training scheme. A single hidden layer was considered in these models. The number of neurons in the hidden layer were subjected to trials (varied from 9 to 12) and the one producing the most accurate results was selected. The trained values of connecting weights and bias for the three models obtained from the FFBP training scheme, discussed in earlier sections, are given in Tables 6–8. It is worth mentioning here that the data of the variables used in the above analysis is well spread, as discussed in Sec. 4, which justifies its use for development of ANN model. Moreover, the testing and training errors also converged to about the same value.

The predicted values of the residual strength of concrete have been plotted against its observed values in Fig. 8 (Fig. 8(a) and (c) and 8(e)) for the three models. The histogram of error for the three models is plotted in Fig. 9.

Table 6
Connection weights and biases for Model-ANN1-R used for the prediction of residual strength of concrete containing calcareous aggregates after exposure to elevated temperature (Transfer functions: tansig and purelin; Output layer bias, b_2 = 0.1901 for predictive model and 0.1422 for design model and R^2 = 0.842).

Neuron	Input hidden layer weights, W_1		Input hidden layer bias, b_1	Output layer weight, W_2	
	w/b	T		Predictive model	Design model
1	−0.4466	−0.2878	5.5232	−0.9290	−0.6948
2	2.2171	−2.9698	−5.0495	5.0032	3.7421
3	−3.8614	−6.6438	−8.7686	−0.5292	−0.3958
4	6.7189	−5.9739	−5.2051	1.0264	0.7677
5	3.4807	−3.3420	−0.3145	1.7405	1.3018
6	−4.8072	5.0317	−2.6555	−2.2113	−1.6539
7	1.7104	−1.7856	0.8792	−3.4050	−2.5468
8	2.0091	−1.1153	2.5969	2.2120	1.6544
9	−5.0565	7.4846	−14.6124	−1.0513	−0.7863
10	−2.5997	3.8963	5.7002	2.8384	2.1230
11	4.8363	1.3102	8.8458	0.7530	0.5632
w/b	–	–	–	−3.0045	−2.2472
T	–	–	–	1.1755	0.8792

w/b = water to binder ratio; T = elevated temperature; R^2 = coefficient of determination.

Table 7
Connection weights and biases for Model-ANN2-R used for the prediction of residual strength of concrete containing siliceous aggregates after exposure to elevated temperature (Transfer functions: tansig and purelin; Output layer bias, b_2 = 0.8969 for predictive model and 0.6555 for the design model and R^2= 0.935).

Neuron	Input hidden layer weights, W_1			Input hidden layer bias, b_1	Output layer weight, W_2	
	a/b	*w/b*	*T*		Predictive model	Design model
1	−1.3225	0.8415	−1.0385	3.2821	−1.0836	−0.7919
2	0.5996	0.8965	0.1891	−1.2902	−0.7241	−0.5292
3	0.9175	1.1825	0.5687	−2.2447	0.3461	0.2530
4	−0.4807	−0.3903	−0.8234	2.1073	−0.2696	−0.1970
5	1.0244	−0.6252	0.9568	0.1243	0.5742	0.4197
6	−0.4295	−1.5036	0.0589	−0.1472	1.1017	0.8052
7	−0.2317	2.0310	0.1115	−1.4814	−0.0818	−0.0598
8	−0.4934	−0.3938	−1.7275	1.9605	0.2357	0.1723
9	−1.4677	0.8105	0.4306	−2.6040	−0.1510	−0.1104
10	0.7792	−0.8443	0.6606	2.7238	0.4578	0.3346
11	0.0912	−1.3044	−1.0103	4.2386	−0.6226	−0.4551
a/b	–	–	–	–	−0.4018	−0.2936
w/b	–	–	–	–	0.4081	0.2983
T	–	–	–	–	−0.4343	−0.3174

a/b = aggregate to binder ratio; *w/b* = water to binder ratio; *T* = elevated temperature; R^2 = coefficient of determination.

Table 8
Connection weights and biases for Model-ANN3-R used for the prediction of residual strength of concrete for all aggregate types after exposure to elevated temperature (Transfer functions: tansig and purelin; Output layer bias, b_2 = 1.4029 for predictive model and 0.9648 for the design model and R^2= 0.868).

Neuron	Input hidden layer weights, W_1			Input hidden layer bias, b_1	Output layer weight, W_2	
	w/b	*T*	$f'_{c,R}$		Predictive model	Design model
1	−0.2894	−0.9246	−0.8526	2.2059	−1.9272	−1.3254
2	0.1861	−3.9572	−2.6736	−7.3501	0.7102	0.4884
3	2.5135	−2.5631	3.4518	−8.5465	0.7539	0.5185
4	0.6275	0.3745	−1.8343	1.2015	−1.2731	−0.8756
5	0.4641	3.0506	5.2060	−1.3363	0.3583	0.2464
6	3.5866	−1.4201	9.8295	−3.0586	0.3896	0.2679
7	−1.6766	0.5765	1.7605	−1.1461	−0.8417	−0.5788
8	0.9762	−0.9718	−0.5809	−1.3730	0.8705	0.5987
9	0.6577	0.1696	3.5961	2.3825	0.7964	0.5477
10	−0.1151	−1.2329	−0.1752	−1.8888	−2.8286	−1.9453
w/b	–	–	–	–	−1.1571	−0.7958
T	–	–	–	–	−1.3353	−0.9183
$f'_{c,R}$	–	–	–	–	−2.0313	−1.3970

w/b = water to binder ratio; *T* = elevated temperature; $f'_{c,R}$ = compressive strength of concrete at room temperature; R^2 = coefficient of determination.

The values of the error estimates for the predictive models are reported in Table 9, which show good correlation for all the three models. As given in Table 9, the mean errors in neural network models ANN1-R, ANN2-R, and ANN3-R are 12.5%, 13.1%, and 17.2%, respectively. For the three models respectively, 71.2%, 66.7% and 61.5% data has error less than 15%. It is also observed that for 80% of the data, the percentage error is less than 19.3%, 22.3%, and 25.5% for the three models respectively. Additionally, the ANN models featured small RMSE during training; however, the value was slightly higher during validation. All the models showed consistently good correlation throughout the training and testing.

7.1. Proposed ANN design models

The ANN models, given by Eqs. (8)–(10), are transformed into the design models by incorporating a safety factor (or reduction factor). Due to the brittle nature of concrete after exposure to elevated temperature, which is to be avoided, the reduction factor for the residual strength calculations is based on statistical lower bounds of the ratio of experimental to the predicted shear strength in terms of *mean* − 2σ, where σ is the standard deviation [37,38,95]. For deciding the design safety factor for the residual strength of HSC, two more conditions were enforced – a maximum of 5% non-conservative data points and a minimum safety factor of 1.00 for 95% of the data. The reduction factors obtained by trial for satisfying these conditions for the three design models ANN1-RD, ANN2-RD, and ANN3-RD corresponding to the three predictive models (ANN1-R, ANN2-R, and ANN3-R) were 0.748, 0.731, and 0.688 respectively. The incorporation of these factors in the model causes some changes in the output biases and weights of the models. The modified values of the output layer weight, W_2, and bias b_2, for the three models are reported in Tables 6–8 However, the hidden layer weight and bias remain unchanged, as given in these tables.

A comparison of the experimental and predicted values of the residual strength of concrete for the three recommended ANN design models is also shown in Fig. 8(b) and (d) and 8(f). The plots without the employment of the reduction factor are already plotted in this figure (Fig. 8(a) and (c) and 8(e)) for clearly showing the scatter in their prediction.

The spread of quartiles of the deviations in the prediction of residual strength of concrete is depicted in Fig. 10. This plot provides an overall picture of the scatter in the prediction of residual concrete strength by different models. The positive deviation indicates non-conservative prediction because of the prediction being higher than the experimental value. The bottom and top ends of the bars represent respectively the lower limit and the upper limit of the deviations. For the best performing model, the full height of deviation bar should lie under the zero deviation line, and the 2nd and 3rd quartiles as well as the total height of vertical bar are minimum. All these desired ideal characteristics are best met by the proposed ANN models.

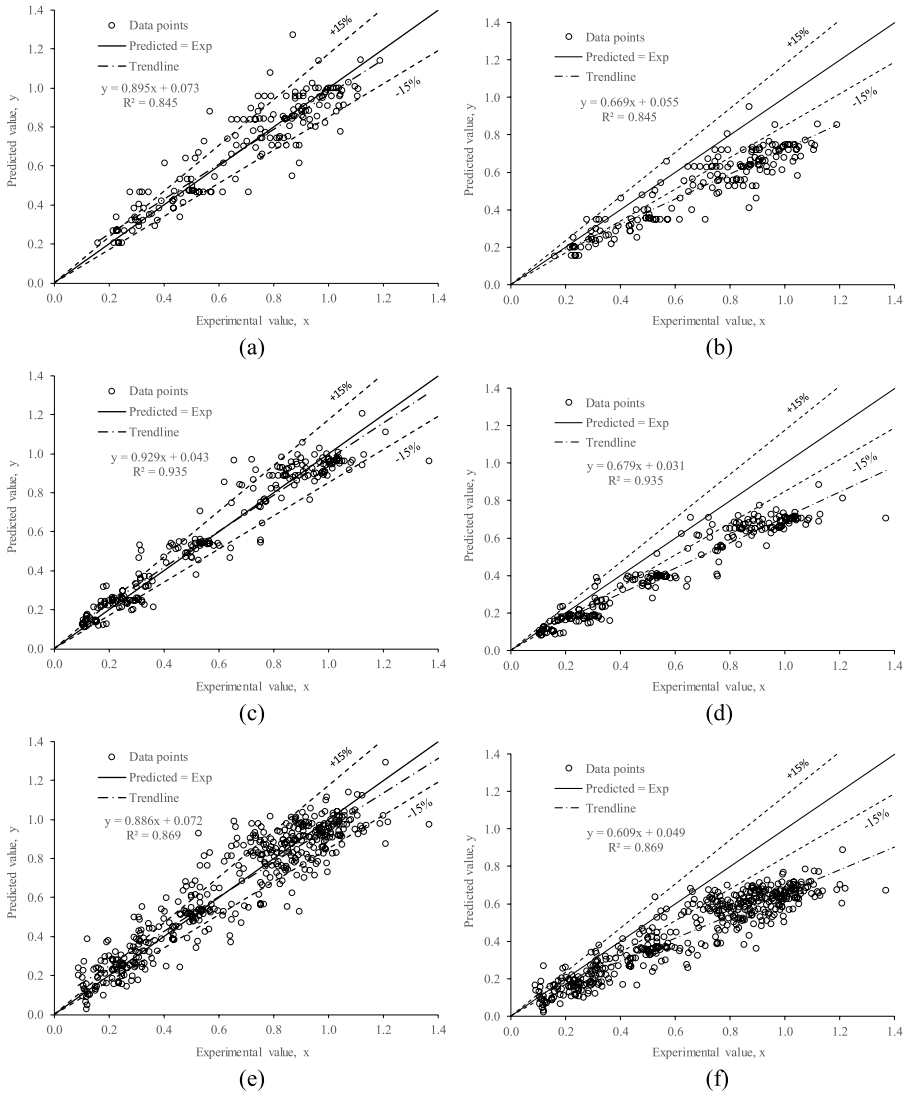

Fig. 8. Comparison of residual strength prediction by proposed ANN models with experiment: (a) Predictive model ANN1-R for calcareous aggregates; (b) Design model ANN1-RD for calcareous aggregates; (c) Predictive model ANN2-R for siliceous aggregates; (d) Design model ANN2-RD for siliceous aggregates; (e) Predictive model ANN3-R for all aggregates; and (f) Design model ANN3-RD for all aggregates.

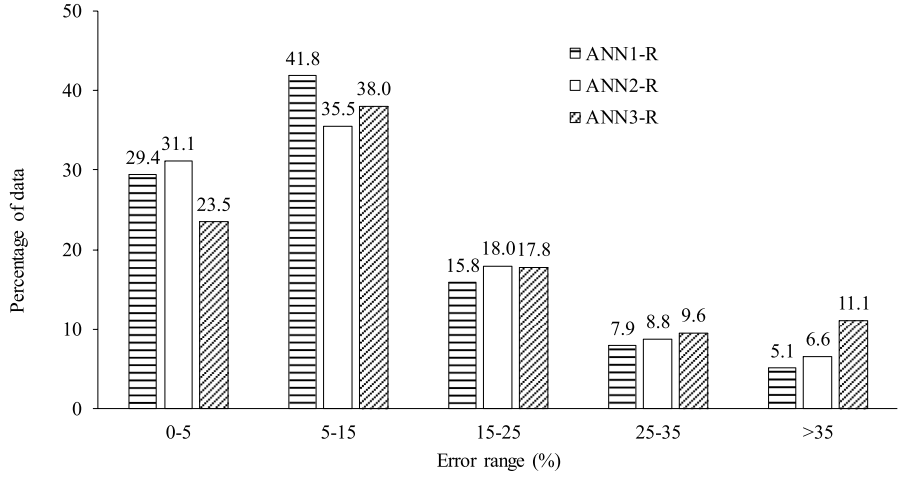

Fig. 9. Histogram of error in the prediction of residual strength of concrete by ANN predictive models.

Table 9
Error estimates for different predictive ANN models.

Parameter for Error Estimate	Relative concrete strength (R = $f'_{c,T}/f'_{c,R}$)		
	ANN1-R	ANN2-R	ANN3-R
Mean percent error (MPE)	1.95	3.35	3.18
Mean absolute percent error (MAPE)	12.5	13.1	17.2
Root mean square error (RMSE)	0.10	0.08	0.11
Correlation coefficient (CC)	0.919	0.967	0.932
Percent data for error within 15%	71.2	66.7	61.5
Percentage error enveloping 80% data	19.3	22.3	25.5

$f'_{c,R}$ = compressive strength of concrete at room temperature; $f'_{c,T}$ = residual compressive strength of concrete after exposure to temperature T.

The ratio of experimental to the predicted value of residual strength of concrete was calculated for checking the accuracy of different models. The models were assessed on the basis of the statistical parameters such as coefficient of variation (CV), SD and mean, whose values are reported in Table 10. The percentage of non-conservative data and 5th percentile of the ratio of experimental to predicted value is also given in the table. The best model would be one for which, SD and CV are small, mean is more than 1 but close to unity, 5th percentile is at least 1.00 and there are almost no non-conservative data points.

All the three models of different codes of practice are non-conservative but the non-conservative data for ACI 216.1–07 [5] and Eurocode 2: EN 1992-1-2 [4] is low which is 17.9% and 25.8%, for the two models respectively. The prediction model of ASCE Manual [6] is the most non-conservative in predicting residual concrete strength with 66% non-conservative data points. However, the prediction of ACI 216.1–07 [5] is better among the three models of the codes. On the other hand, among the six models of different researchers, Phan and Carino (2003) and Choe et al. (2015) are better than the rest of the models with the non-conservative data for the two models being 7.6% and 12.4%, respectively. Although all other models are non-conservative, Aslani and Bastami (2011) is the most non-conservative model with 41.4% non-conservative prediction. It is discernible from Table 10 that the recommended ANN design models are the best among all the models presented in the table. The value of the 5th percentile for all the three recommended ANN based design models is 1.0, thus meeting the target of its minimum value as 1.0. It is worth mentioning here that the proposed models are only empirical and not physical.

Since most of the experimental data used in this study is for $f'_{c,R}$ up to 100 MPa (about 96.0%), it is recommended that the proposed design models be limited to the compressive strength of concrete not more than 100 MPa. For concrete strength exceeding 100 MPa, $f'_{c,R}$ should be taken as 100 MPa. In future, when more data for higher concrete strength and steel ratio are available, these models may be checked and revised, if necessary, to increase the limits of their applicability.

8. Conclusions

- The data collected from literature was analyzed statistically to ascertain the impact of different independent variables on the unstressed residual strength of HSC after exposure to elevated temperature.
- ANN based models have been developed for predicting the residual strength of concrete after exposure to elevated temperature. The design models were also proposed by modifying the predictive ANN based models. Separate models are developed for concrete containing calcareous and siliceous aggregates. A combined model by considering all aggregate types is also developed. This model can be used when the aggregate type is not known. The network predictions were generally satisfactory.
- The neural network with single hidden layers was selected as the optimum network to predict the residual strength of concrete. The network configuration of the models with FFBP is recommended for general use in order to predict the residual strength of concrete.
- The variables to be included in the model were decided based on the sensitivity analysis, which employed neural network approach as well as statistical methods. For calcareous aggregates, water to binder ratio and elevated temperature were included in the model, whereas for siliceous aggregates, besides these variables, aggregate to binder ratio was also included. The water to binder ratio, elevated temperature, and the compressive strength of concrete were the most significant variables showing correlation and were thus included in the development of the model for all aggregates. The ANN models featured small errors and consistently good correlation.

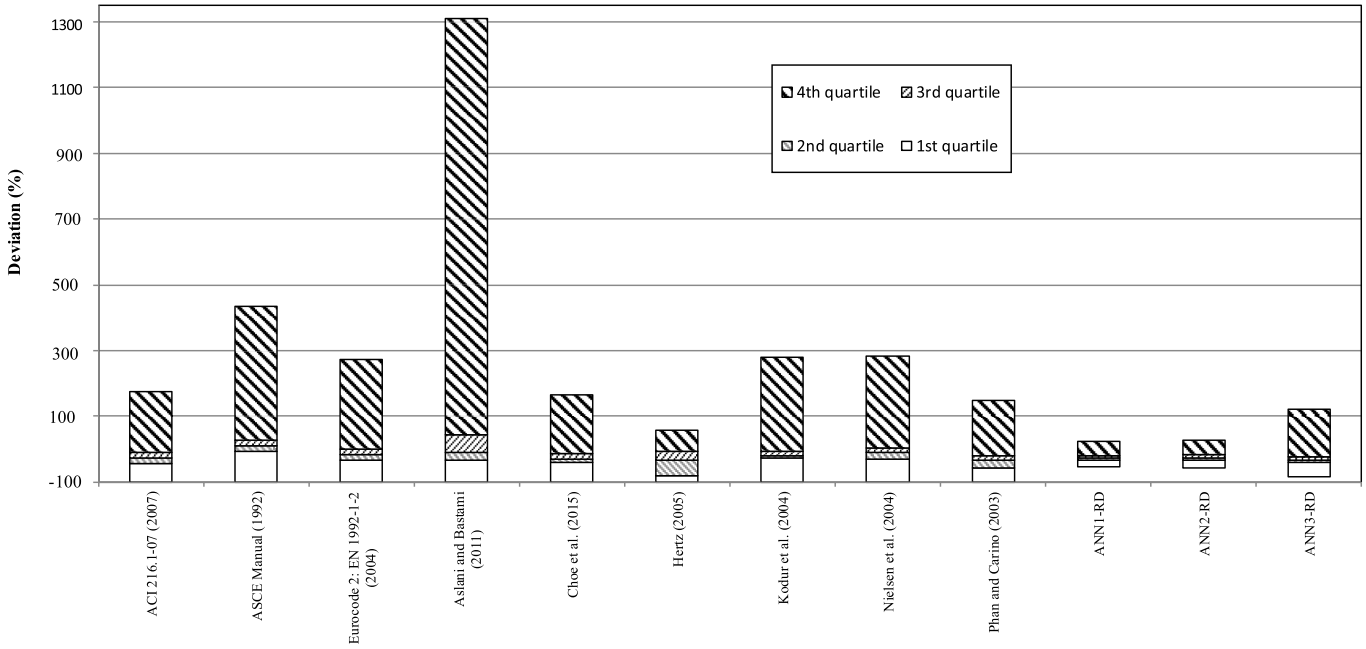

Fig. 10. Comparison of spread of quartiles of error percentiles for different models.

Table 10
Statistical parameters for the assessment of models (460 data points).

Model	Statistical parameters for experimental to predicted ratio[a]								Non-conservative data (%)
	Mean	SD	CV (%)	5th percentile value	Min. value	Max. value	CC	R^2	
Predictive Models									
Model ANN1-R	1.01	0.16	15.9	0.75	0.60	1.59	0.92	0.84	–
Model ANN2-R	1.00	0.17	17.2	0.73	0.57	1.70	0.97	0.94	–
Model ANN3-R	1.03	0.28	27.5	0.69	0.31	4.47	0.93	0.87	–
Design Models									
Model ANN1-RD	1.35	0.21	15.9	1.00	0.80	2.12	0.92	0.84	5.1
Model ANN2-RD	1.36	0.23	17.2	1.00	0.79	2.32	0.97	0.94	5.3
Model ANN3-RD	1.49	0.41	27.5	1.00	0.45	6.50	0.93	0.87	5.0
Eurocode 2: EN 1992-1-2 (2004)	1.31	0.80	60.7	0.68	0.27	15.09	0.83	0.69	25.8
ACI 216.1–07 (2007)	1.44	1.10	76.4	0.81	0.36	14.54	0.87	0.76	17.9
ASCE Manual (1992)	0.94	0.31	32.6	0.50	0.19	2.50	0.87	0.75	66.0
Kodur et al. (2004)	1.23	0.42	34.0	0.71	0.26	6.42	0.88	0.78	19.4
Nielsen et al. (2004)	1.67	1.99	119.8	0.68	0.26	9.71	0.89	0.79	31.1
Aslani and Bastami (2011)	1.08	0.60	55.4	0.15	0.07	3.60	0.17	0.03	41.4
Choe et al. (2015)	1.58	0.96	60.9	0.90	0.38	9.05	0.88	0.77	12.4
Phan and Carino (2003)	1.57	0.90	57.5	0.91	0.40	10.37	0.89	0.79	7.6
Hertz (2005)	2.15	1.95	90.7	0.80	0.63	10.00	0.87	0.75	18.6

[a] Data for zero predicted value was excluded; SD = standard deviation; CV = coefficient of variation; CC = coefficient of correlation; R^2 = coefficient of determination.

Conflicts of interest

The authors declare that they have no conflict of interest.

Acknowledgements

This research was supported by Deanship of Scientific Research Chairs at King Saud University, Saudi Arabia for Chair of Research and Studies in Strengthening and Rehabilitation of Structures at Civil Engineering Department.

Appendix A. Supplementary data

Supplementary data to this article can be found online at https://doi.org/10.1016/j.firesaf.2019.03.011.

Nomenclature

a/b	aggregate to binder ratio
$f'_{c,R}$	compressive strength of concrete at room temperature
$f'_{c,T}$	residual compressive strength of concrete after exposure to temperature
h	soaking period
H_r	heating rate
$n1$, $n2$	number of neurons
p, q, s, and u	model parameters
T	elevated temperature in °C
w/b	water to binder ratio
R	ratio of residual compressive strength to the compressive strength of concrete at room temperature
R^2	coefficient of determination
CC	coefficient of correlation
CFBP	cascade-forward back propagation
CV	coefficient of variation
EBP	Elman back propagation
FFBP	feed-forward back propagation
MAPE	mean absolute percent error
MPE	mean percent error
RMSE	root mean square error
SD	standard deviation

References

[1] N. Subramanian, Evaluation and enhancing the punching shear resistance of flat slabs using HSC, Indian Concr. J. 79 (4) (2005) 31–37 2005.
[2] American Concrete Institute (ACI), Report on High-Strength Concrete, American Concrete Institute, Detroit, MI, USA, 2010 ACI 363R-10.
[3] M. Hamrat, B. Boulekbache, M. Chemrouk, S. Amziane, Shear behaviour of RC beams without stirrups made of normal strength and high strength concretes, Adv. Struct. Eng. 13 (1) (2010) 29–41.
[4] Comité Européen de Normalisation (CEN), EN 1992-1-2: Eurocode 2: Design of Concrete Structures - Part 1-2: General Rules - Structural Fire Design, (2004) Brussels, Belgium, 100 pp.
[5] Joint ACI-TMS Committee 216, Code Requirements for Determining Fire Resistance of Concrete and Masonry Construction Assemblies (ACI-TMS 216.1-07), Farmington Hills, MI, 2007 28 pp.
[6] ASCE Committee on Fire Protection, "Structural Fire Protection: Manual of Practice," Manual and Report No. 78, American Society of Civil Engineers, Structural Division, New York, NY, 1992 260 pp.
[7] H. Elsanadedy, T. Almusallam, Y. Al-Salloum, R. Iqbal, Effect of high temperature on structural response of reinforced concrete circular columns strengthened with fiber reinforced polymer composites, J. Compos. Mater. 51 (3) (2017) 333–355 Sage Publications.
[8] C. Zhai, L. Chen, Q. Fang, W. Chen, X. Jiang, Experimental study of strain rate effects on normal weight concrete after exposure to elevated temperature, Mater. Struct. 50 (2017) 40.
[9] T. Drzymała, W. Jackiewicz-Rek, M. Tomaszewski, A. Kuś, J. Gałaj, R. Šukys, Effects of high temperature on the properties of high performance concrete (HPC), Procedia Eng. 172 (2017) 256–263.
[10] T. Gupta, S. Siddique, R.K. Sharma, S. Chaudhary, Effect of elevated temperature and cooling regimes on mechanical and durability properties of concrete containing waste rubber fiber, Constr. Build. Mater. 137 (2017) 35–45.
[11] İ. Türkmen, A.F. Bingöl, A. Tortum, R. Demirboğa, R. Gül, Properties of pumice aggregate concretes at elevated temperatures and comparison with ANN models, Fire Mater. 41 (2017) 142–153.
[12] Y.A. Al-Salloum, T.H. Almusallam, H.M. Elsanadedy, R.A. Iqbal, Effect of elevated temperature environments on the residual axial capacity of RC columns strengthened with different techniques, Constr. Build. Mater. 115 (2016) 345–361.
[13] J. Huo, B. Jin, Q. Yu, Y. He, Y. Liu, Effect of microstructure variation on damage evolution of concrete at high temperatures, ACI Mater. J. 113 (5) (2016) 547–558.
[14] Y.A. Al-Salloum, H.M. Elsanadedy, A.A. Abadel, Behavior of FRP-confined concrete after high temperature exposure, Constr. Build. Mater. 25 (2) (2011) 838–850.
[15] L.T. Phan, N.J. Carino, Fire performance of high strength concrete: research needs, Proceedings of ASCE/SEI Structures Congress, May 8-10, 2000, Philadelphia, PA, 2000.
[16] M.S. Abrams, Compressive Strength of Concrete at Temperatures to 1600 °F, American Concrete Institute (ACI) SP 25, Temperature and Concrete, Detroit, Michigan, 1971.
[17] C. Castillo, A.J. Durrani, Effect of transient high temperature on high-strength concrete, ACI Mater. J. 87 (1) (1990) 47–53.
[18] U. Diederichs, U.M. Jumppanen, V. Penttala, Material properties of high strength concrete at elevated temperatures, IABSE 13th Congress, Helsinki, June 1988, 1988.
[19] U. Diederichs, U.M. Jumppanen, V. Penttala, Behavior of High Strength Concrete at High Temperatures, Helsinki University of Technology, Department of Structural Engineering, 1989 Report #92.

[20] K. Hertz, Danish investigations on silica fume concretes at elevated temperatures, Proceedings of ACI 1991 Spring Convention, Boston, MA, March 17-21, 1991, 1991.
[21] G. Khoury, S. Algar, Mechanical behavior of HPC and UHPC concretes at high temperatures in compression and tension, Paper Presented at ACI International Conference on State-Of-The-Art in High Performance Concrete, Chicago, Illinois, March 1999, 1999.
[22] H.L. Malhotra, The effect of temperature on the compressive strength of concrete, Mag. Concr. Res. 8 (22) (1956) 85–94.
[23] L.T. Phan, J.R. Lawson, F.L. Davis, Effects of elevated temperature exposure on heating characteristics, spalling, and residual properties of high performance concrete, RILEM Mater. Structr. J. 34 (2001) 83–91.
[24] U. Schneider, Concrete at high temperatures - a general review, Fire Saf. J. (1988) 55–68. The Netherlands.
[25] P.J.E. Sullivan, R. Sharshar, Performance of concrete at elevated temperatures (as measured by the reduction in compressive strength), Fire Technol. 28 (3) (1992) 240–250.
[26] L.T. Phan, "Fire Performance of High-Strength Concrete: A Report of the State-Of-The-Art," NISTIR 5934, Building and Fire Research Laboratory, National Institute of Standards and Technology, Gaithersburg, Maryland, 1996.
[27] L.T. Phan, N.J. Carino, Review of mechanical properties of HSC at elevated temperature, J. Mater. Civil Eng. ASCE 10 (1) (1998) 58–64.
[28] V.K.R. Kodur, T.C. Wang, F.P. Cheng, Predicting the fire resistance behaviour of high strength concrete columns, Cement Concr. Compos. 26 (2004) 141–153.
[29] C.V. Nielsen, C.J. Pearce, N. Bicanic, Improved phenomenological modeling of transient thermal strains for concrete at high temperature, Comput. Concr. 1 (2) (2004) 189–209.
[30] F. Aslani, M. Bastami, Constitutive relationships for normal- and high-strength concrete at elevated temperatures, ACI Mater. J. 108 (4) (2011) 355–364.
[31] G. Choe, G. Kim, N. Gucunski, S. Lee, Evaluation of the mechanical properties of 200 MPa ultra-high-strength concrete at elevated temperatures and residual strength of column, Constr. Build. Mater. 86 (2015) 159–168.
[32] L.T. Phan, N.J. Carino, Code provisions for high strength concrete strength-temperature relationship at elevated temperatures, Mater. Struct. 36 (2003) 91–98.
[33] K.D. Hertz, Concrete strength for fire safety design, Mag. Concr. Res. 57 (8) (2005) 445–453.
[34] M. Hosseini, H. Abbas, Neural network approach for estimation of hole-diameter in thin plates perforated by spherical projectiles, Thin-Walled Struct. 46 (6) (2008) 592–601.
[35] A.A. Shah, H. Abbas, S.H. Alsayed, Y.A. Al-Salloum, T.H. Almusallam, Predicting residual strength of non-linear ultrasonically evaluated damaged concrete using artificial neural network, Constr. Build. Mater. 29 (2012) 42–50.
[36] H.M. Elsanadedy, Y.A. Al-Salloum, H. Abbas, S.H. Alsayed, Prediction of strength parameters of FRP confined concrete, Compos. B Eng. 43 (2012) 228–239.
[37] H.M. Elsanadedy, H. Abbas, Y.A. Al-Salloum, T.H. Almusallam, Prediction of intermediate crack debonding strain of externally bonded FRP laminates in RC beams and one-way slabs, J. Compos. Constr. 18 (5) (2014), https://doi.org/10.1061/(ASCE)CC.1943-5614.0000462 Published online.
[38] H.M. Elsanadedy, H. Abbas, Y.A. Al-Salloum, T.H. Almusallam, Shear strength prediction of HSC slender beams without web reinforcement, Mater. Struct. 49 (9) (2016) 3749–3772, https://doi.org/10.1617/s11527-015-0752-x Sept. 2016.
[39] L. Liu, Fire Performance of High Strength Concrete Materials and Structural Concrete, Ph.D. Thesis Florida Atlantic University, Boca Raton, Florida, USA, 2009.
[40] K.D. Caple, A Pilot Study on the Effects of Temperature on the Material Properties of Prestressed Concrete and the Use of Thermogravimetric Analysis in the Assessment of Heat-Affected Concrete, M.Sc. Thesis Clemson University, South Carolina, USA, 2007.
[41] G.-F. Peng, Evaluation of Fire Damage to High Performance Concrete, Ph.D. Thesis The Hong Kong Polytechnic University, Hong Kong, 2000.
[42] Y. Xu, Y.L. Wong, C.S. Poon, M. Anson, Impact of high temperature on PFA concrete, Cement Concr. Res. 31 (2001) 1065–1073.
[43] O. Arioz, Retained properties of concrete exposed to high temperatures: size effect, Fire Mater. 33 (2009) 211–222.
[44] D.J. Martins, J.R. Correia, J. de Brito, The effect of high temperature on the residual mechanical performance of concrete made with recycled ceramic coarse aggregates, Fire Mater. 40 (2016) 289–304.
[45] M. Yaqub, C.G. Bailey, Non-destructive evaluation of residual compressive strength of post-heated reinforced concrete columns, Constr. Build. Mater. 120 (2016) 482–493.
[46] L. Biolzi, S. Cattaneo, G. Rosati, Evaluating residual properties of thermally damaged concrete, Cement Concr. Compos. 30 (2008) 907–916.
[47] K.S. Al-Jabri, M.B. Waris, A.H. Al-Saidy, Effect of aggregate and water to cement ratio on concrete properties at elevated temperature, Fire Mater. 40 (2016) 913–925.
[48] E.A. Kerr, Damage Mechanisms and Repairability of High Strength Concrete Exposed to Elevated Temperatures, Ph.D. Thesis University of Notre Dame, Indiana, USA, 2007.
[49] M. Bastami, A. Chaboki-Khiabani, M. Baghbadrani, M. Kordi, Performance of high strength concretes at elevated temperatures, Scientia Iranica, Trans. A: Civ. Eng. 18 (5) (2011) 1028–1036.
[50] M. Bastami, M. Baghbadrani, F. Aslani, Performance of nano-Silica modified high strength concrete at elevated Temperatures, Constr. Build. Mater. 68 (2014) 402–408.
[51] K.K. Sideris, P. Manita, Residual mechanical characteristics and spalling resistance of fiber reinforced self-compacting concretes exposed to elevated temperatures, Constr. Build. Mater. 41 (2013) 296–302.
[52] E. Tolentino, F.S. Lameiras, A.M. Gomes, C.A. Rigo da Silva, W.L. Vasconcelos, Effects of high temperature on the residual performance of Portland cement concretes, Mater. Res. 5 (3) (2002) 301–307.
[53] R. Felicetti, P.G. Gambarova, M.P. Natali Sora, G.A. Khoury, Mechanical behaviour of HPC and UHPC in direct tension at high temperature and after cooling, Proc. 5th Symposium on Fibre-Reinforced Concrete BEFIB 2000, Lyon (France), September 13-15, 2000, pp. 749–758.
[54] I. Hager, T. Tracz, J. Śliwiński, K. Krzemień, The influence of aggregate type on the physical and mechanical properties of high-performance concrete subjected to high temperature, Fire Mater. 40 (2016) 668–682.
[55] J. Lee, K. Choi, K. Hong, B.H. Oh, et al. (Ed.), "The Effect of High Temperature on Color and Residual Compressive Strength of Concrete," Proceedings of Fracture Mechanics of Concrete and Concrete Structures (FraMCoS-7), May 23-28, South Korea, 2010, pp. 1772–1775.
[56] A.H. Ahmad, O.M. Abdulkareem, Effect of high temperature on mechanical properties of concrete containing admixtures, Al-Rafidain Eng.J.Iraq 18 (4) (2010) 43–54.
[57] S.H. Chowdhury, S.T. Smith (Ed.), Effect of Elevated Temperature on Mechanical Properties of High Strength Concrete," 23rd Australasian Conference on the Mechanics of Structures and Materials (ACMSM23), Byron Bay, Australia, 9-12 December, 2014, pp. 1077–1082.
[58] C.B.K. Rao, R. Kumar, A study on behaviour of normal strength concrete and high strength concrete subjected to elevated temperatures, Int. J. Civ. Environ., Struct. Constr. Arch. Eng. 9 (3) (2015) 283–287.
[59] A. Lau, Effect of High Temperatures on Normal Strength Concrete and High Performance Concrete Containing Steel Fibers, Ph.M. Thesis The Hong Kong Polytechnic University, Hong Kong, 2003.
[60] J.A. Purkiss, Steel fibre reinforced concrete at elevated temperatures, Int. J. Cem. Compos. Lightweight Concr. 6 (3) (1984) 179–184.
[61] I. Netinger, M.J. Rukavina, A. Mladenovic, Improvement of post-fire properties of concrete with steel slag aggregate, Procedia Eng. 62 (2013) 745–753.
[62] B. Toumi, M. Resheidat, Z. Guemmadi, H. Chabil, Coupled effect of high temperature and heating time on the residual strength of normal and high-strength concretes, Jordan J. Civ. Eng. 3 (4) (2009) 322–330.
[63] M. Uysal, H. Tanyildizi, Estimation of compressive strength of self compacting concrete containing polypropylene fiber and mineral additives exposed to high temperature using artificial neural network, Constr. Build. Mater. 27 (2012) 404–414.
[64] S. Hachemi, A. Ounis, S. Chabi, Evaluating residual mechanical and physical properties of concrete at elevated temperatures, Int. J. Civ. Environ., Struct. Constr. Arch. Eng. 8 (2) (2014) 176–181.
[65] A. Noumowe, C. Galle, Study of high strength concretes at raised temperature up to 200 °c: thermal gradient and mechanical behaviour, International Association for Structural Mechanics in Reactor Technology (IASMiRT), SMiRT 16 Conf., Washington DC. August 12-17, 2001, pp. 1–8 Paper # 1580.
[66] Y.N. Chan, G.F. Peng, M. Anson, Residual strength and pore structure of high-strength concrete and normal strength concrete after exposure to high temperatures, Cement Concr. Compos. 21 (1999) 23–27.
[67] B. Demirel, O. Kelestemur, Effect of elevated temperature on the mechanical properties of concrete produced with finely ground pumice and silica fume, Fire Saf. J. 45 (2010) 385–391.
[68] N. Anagnostopoulos, K.K. Sideris, A. Georgiadis, Mechanical characteristics of self-compacting concretes with different filler materials, exposed to elevated temperatures, Mater. Struct. 42 (2009) 1393–1405.
[69] O. Arioz, Effects of elevated temperatures on properties of concrete, Fire Saf. J. 42 (2007) 516–522.
[70] A. Behnood, M. Ghandehari, Comparison of compressive and splitting tensile strength of high-strength concrete with and without polypropylene fibers heated to high temperatures, Fire Saf. J. 44 (2009) 1015–1022.
[71] Z. Bin Johari, Mechanical Properties of High Strength Concrete at High Temperature Loading, M.Sc. Thesis Universiti Tecknologi Malaysia, 2005.
[72] M.S. Cülfik, T. Özturan, Mechanical properties of normal and high strength concretes subjected to high temperatures and using image analysis to detect bond deteriorations, Constr. Build. Mater. 24 (2010) 1486–1493.
[73] Y. Esen, The effect of cure conditions and temperature changes on the compressive strength of normal and fly ash added concretes, Int. J. Phys. Sci. 5 (17) (2010) 2598–2604.
[74] D. Campbell-Allen, E.W.E. Low, H. Roper, An investigation on the effect of elevated temperatures on concrete for reactor vessels, Nucl. Struct. Eng. 2 (1965) 382–388.
[75] K. Hertz, "Heat-induced Explosion of Dense Concrete," Report No. 166, Institute of Building Design, Technical University of Denmark, 1984.
[76] M.S. Khan, H. Abbas, Performance of concrete subjected to elevated temperature, Eur. J. Environ. Civ. Eng. 20 (5) (2016) 532–543.
[77] M. Khandaker, A. Hossain, High strength blended cement concrete incorporating volcanic ash: performance at high temperatures, Cement Concr. Compos. 28 (2006) 535–545.
[78] A. Noumowé, Mechanical properties and microstructure of high strength concrete containing polypropylene fibres exposed to temperatures up to 200 °C, Cement Concr. Res. 35 (2005) 2192–2198.
[79] A. Noumowé, H. Carré, A. Daoud, H. Toutanji, High-strength self-compacting concrete exposed to fire test, J. Mater. Civil Eng. ASCE 18 (6) (2006) 754–758.
[80] C.S. Poon, Z.H. Shui, L. Lam, Compressive behavior of fiber reinforced high-performance concrete subjected to elevated temperatures, Cement Concr. Res. 34 (2004) 2215–2222.
[81] A. Savva, P. Manita, K.K. Sideris, Influence of elevated temperatures on the mechanical properties of blended cement concretes prepared with limestone and siliceous aggregates, Cement Concr. Compos. 27 (2005) 239–248.

[82] F.U.A. Shaikh, V. Vimonsatit, Effect of cooling methods on residual compressive strength and cracking behavior of fly ash concretes exposed at elevated temperatures, Fire Mater. 40 (2016) 335–350.
[83] J. Xiao, H. Falkner, On residual strength of high-performance concrete with and without polypropylene fibres at elevated temperatures, Fire Saf. J. 41 (2006) 115–121.
[84] C.J. Zega, A.A. Di Maio, Recycled concrete made with different natural coarse aggregates exposed to high temperature, Constr. Build. Mater. 23 (2009) 2047–2052.
[85] J. Geng, Q. Sun, W. Zhang, C. Lü, Effect of high temperature on mechanical and acoustic emission properties of calcareous-aggregate concrete, Appl. Therm. Eng. 106 (2016) 1200–1208.
[86] T. Morita, H. Saito, H. Kumagai, Residual mechanical properties of high strength concrete members exposed to high temperature – Part 1. Test on material properties, Summaries of Technical Papers of Annual Meeting, Architectural Institute of Japan, Niigata, August, 1992(in Japanese).
[87] Z. Xing, A.-L. Beaucour, R. Hebert, A. Noumowe, B. Ledesert, Influence of the nature of aggregates on the behaviour of concrete subjected to elevated temperature, Cement Concr. Res. 41 (2011) 392–402.
[88] H.-S. Shang, T.-H. Yi, Behavior of HPC with fly ash after elevated temperature, Adv. Mater. Sci. Eng. 2013 (2013), https://doi.org/10.1155/2013/478421 Article ID 478421, 7 pages.
[89] S.-T. Yi, E.-I. Yang, J.-C. Choi, Effect of specimen sizes, specimen shapes, and placement directions on compressive strength of concrete, Nucl. Eng. Des. 236 (2006) 115–127.
[90] ULC. CAN/ULC-S101-M04, Standard Methods of Fire Endurance Tests of Building Construction and Materials. Scarborough, Ont, Underwriters' Laboratories of Canada, 2004.
[91] ASTM. ASTM E119-01, Standard Methods of Fire Test of Building Construction and Materials, American Society for Testing and Materials, West Conshohocken, PA, 2001.
[92] ISO, Fire-resistance Tests – Elements of Building Construction – Part 1: General Requirements, International Organization for Standardization, Geneva, Switzerland, 1999 ISO 834-1:1999.
[93] Y.A. Al-Salloum, A.A. Shah, H. Abbas, S.H. Alsayed, T.H. Almusallam, M.S. Al-Haddad, Prediction of compressive strength of concrete using neural networks, Comput. Concr. 10 (2) (2012) 197–217.
[94] C.J. Kowalski, On the effects of non-normality on the distribution of the sample product-moment correlation coefficient, Appl. Stat. (1972) 1–12.
[95] H.M. Elsanadedy, M.A. Haroun, Seismic design guidelines for squat composite-jacketed circular and rectangular reinforced concrete bridge columns, ACI Struct. J. 102 (4) (2005) 505–514.